Microfluid Nanofluid (2014) 17:73–84
DOI 10.1007/s10404-013-1286-6

RESEARCH PAPER

Structural instability of an oscillating superparamagnetic micro-bead chain

He-Ching Lin · Yan-Hom Li · Ching-Yao Chen

Received: 9 July 2013 / Accepted: 28 October 2013 / Published online: 12 November 2013

Abstract Issues concerning the structural instability of an oscillating micro-bead chain are addressed based on systematic experiments. The patterns of rupture are categorized into two distinct regimes, referred to as a weak ductile fracture and a strong ductile fracture. A weak ductile fracture describes a more rigid rupture, which often occurs in a pronounced oscillation driven by strong field strengths. The position of the rupture usually favors toward the two sides of the chain. An interesting phenomenon of a reversed rupture, wherein the ruptured segments oscillate in opposite directions, is observed when there is excessive field strength. An important consequence of the reversed rupture is to cause permanent failure of the chaining structure. On the other hand, a strong ductile fracture, featuring significant deformation before rupture, is favored in a more viscous solvent fluid. The positions of the breakages in this regime favor the central region of the chain. The prominence of rupture instability is enhanced by a weaker directional field or by a longer chain, which is in agreement with quantitative assessments by the normal forces acting between the interfaces of beads. In addition, results of the present experiments provide further validations of the global criterion for rupture instability given by $Mn^{1/2} * N > 1.7$, where Mn and N, respectively, represent the dimensionless Mason number and the number of beads in the chain.

H.-C. Lin · Y.-H. Li · C.-Y. Chen (✉)
Department of Mechanical Engineering, National Chiao Tung University, Hsinchu 30010, Taiwan, ROC
e-mail: chingyao@mail.nctu.edu.tw

1 Introduction and experimental setups

A magnetorheological (MR) suspension is an artificial and functionalized fluid containing paramagnetic solid particles suspended in a non-magnetic solvent. MR suspension has been actively applied in the so-called magnetofluidics (Nguyen 2012). A popular application is chaining the nano-sized or micro-sized particles as micro-devices to be effectively manipulated by external fields, such as micro-mechanical sensors (Goubault et al. 2003; Cebers 2005), micro-swimmers (Dreyfus et al. 2005; Cebers 2005; Li et al. 2012b, 2013c), micro-mixers (Biswal and Gast 2004; Kang et al. 2007; Roy et al. 2009) and micro-electro-mechanical systems (MEMS) (Petousis et al. 2007; Lacharme et al. 2009; Weddemann et al. 2011; Karle et al. 2011; Wittbracht et al. 2012). The aggregation processes and the dynamics of micro-chains in motion subjected to different field configurations, e.g., a rotational field (Melle et al. 2000, 2002a, b, 2003; Melle and Martin 2003; Vuppu et al. 2003; Biswal and Gast 2004; Cebers and Javaitis 2004; Cebers and Ozols 2006; Erglis et al. 2008; Frka-Petesic et al. 2011; Banerjee et al. 2012) and an oscillating field (Li et al. 2012a, b, 2013a, b, c), have also been subjects of intensive studies.

Driven by the external fields, a magnetic chain in a rotating field either remains in its chaining formation or is ruptured into multiple sub-chains (ruptured segments). A flexible chain can be bent and rotates synchronously with the overall external field under the critical frequency. When an excessive frequency is applied, the dynamics become asynchronous, with back-and-forth motions. It is well understood that the mechanism for chaining instability in a dynamical field involves competition between the induced viscous torque (M^{v}) and the magnetic torque (M^{m}), which define the dimensionless Mason number (Mn).

When a chain composed of N beads is exposed to an overall external field strength H, the magnetic torque, the induced viscous torque and the corresponding Mason number are given as (Biswal and Gast 2004)

$$M^{\mathrm{m}} = \frac{\mu_0}{4\pi}\frac{3m^2N^2}{2(2a)^3}\sin(2\Delta\theta_L), \tag{1}$$

$$M^{\mathrm{v}} = \frac{4\pi a^3 N}{3}\frac{2N^2}{\ln(N/2)}\eta\omega, \tag{2}$$

$$Mn = \frac{32\eta\omega}{\mu_0\chi^2H^2}, \tag{3}$$

where μ_0 and a represent the vacuum permeability and the radius of beads, respectively. The magnetic susceptibility of the magnetic beads and the viscosity of solvent fluid are denoted as χ and η, respectively. The dipolar moment, m, of a single bead is given by $m = \frac{4\pi a^3}{3}\chi H$. The instantaneous angular speed of the chain is expressed as ω, and $\Delta\theta_{\mathrm{L}}$ is phase lag of the chain to the external field. When the parameters exceed certain critical values, rupture occurs within the early transient time, mainly near center of the chain. The critical length for the prevention of a rupture is inversely proportional to the square root of the Mason number. Recently, verified by experimental results, a sophisticated method is developed (Gao et al. 2012), which is capable to accurately determine the dynamics of a rotational particle chain. A new dimensionless parameter R_T (Gao et al. 2012), which includes both effects of the Mason number and length of the chain, is derived to characterize the special region of interest. It is proposed that this dimensionless parameter R_T is the sole control parameter for the dynamics of the rotational bead chain. The magnetic torque is balanced by the viscous torque at $R_T < 1$, so that the bead chain rotates as a rigid rod following the field. On the contrary, the chain appears breaking and reforming behaviors if value of this parameter exceeds unity ($R_T > 1$).

On the other hand, the condition of an oscillating field differs from the rotational field by two major factors, such as its strong transient phenomena and the distinct field configuration. The strong transient phenomena are characterized by significant variations in instantaneous angular speeds and overall field strengths within a period of oscillation. In the conventional rotational cases, the strength of the overall external field is constant, so that the transient behavior occurs only within the initial stage when the chain starts to move. Afterward, the chain commonly rotates with the external field by an identical period. Because of the constant field strength and the known angular speed, important parameters, e.g., the Mason number or the forth mentioned parameter R_T (Gao et al. 2012), can be predetermined. However, in the oscillating cases, the field strength varies significantly with sign changed. The chain would reverse its oscillating orientation after the crossover of the trajectories of the overall external field and the chain (Li et al. 2012a). These facts lead to a strong unsteady motion with both acceleration and deceleration within one period of oscillation. As a result, neither the actual oscillating amplitude nor the exact instantaneous angular speed can be predetermined. It is known the local acceleration or deceleration leads to unsteady forces (Crowe et al. 2012), including the virtual mass effects as well as the so-called Basset force. The virtual mass effect relates to the force required to accelerate the surrounding fluids, while the Basset term describes the force due to the lagging boundary layer development with changing velocity. More details about these unsteady forces can be referred to Crowe et al. (2012). It is believed the strong unsteady effects might result in significant distinctions between the oscillating chain and its rotational counterpart. In addition, the overall field configuration in an oscillating field condition is composed of two components (Li et al. 2012a, 2013a), i.e. the static directional field and the dynamical perpendicular field. The effects of these two components to the structural chaining instability are inconsistent. In general, stable chaining structure is favorable in a stronger directional field strength, while the perpendicular field tends to destabilize the chaining structure. Besides, the interplays between the two components decide the maximum oscillating amplitude and local instantaneous angular speeds. As a result, careful consideration of the field components, rather than the overall field strength applied in a conventional rotational chain, is essential.

To unveil the behaviors of an oscillating chain, Li et al. (2012a) discussed its detailed dynamics, including the synchronicity of the phase angle trajectories between the chain and the overall external field. Under increasing value of the Mason number (Mn) or number of beads consisted in the chain (N), different oscillating behaviors, from rigid body motion, bending distortions to chaining ruptures, had been demonstrated. Verified in certain particular experimental conditions (Li et al. 2012a, 2013a), a criterion of $Mn^{1/2}{*}N \approx 1.7$ was proposed for the prediction of chaining rupture. In a condition of $Mn^{1/2}{*}N < 1.7$, a chain would oscillate periodically as a whole even its chaining structure could be deformed to an S-shape. If the instantaneous value of $Mn^{1/2}{*}N$ exceeds the threshold at around 1.7, the chaining stability can no longer be sustained and point breakages evolved. After breakages, the ruptured segments commonly undergo reattachments and detachments within oscillations. Furthermore, a phenomenon referred to as trajectory shift, which is analogous to the asynchronous forth-and-back behavior in a rotating field, was identified if the instantaneous phase lag is greater than $\pi/2$ (Li et al.

2013a). Using such an oscillating field configuration, a re-dispersible artificial micro-swimmer can be designed by simply chaining beads of different sizes (Li et al. 2012b, 2013c). Swimmers are effectively driven forward, and their swimming orientations are steered by applying the phenomenon of trajectory shift (Li et al. 2013a, c).

In this study, two major issues that affect the chaining instability are emphasized. Even the global criterion that leads to structural fracture of $Mn^{1/2}{*}N > 1.7$ is well verified by quantitative data in particular experimental situations (Li et al. 2012a, 2013a), these experiments were conducted in limited conditions, e.g., a single size of magnetic beads with a diameter $d = 4.5$ μm in distilled water whose viscosity is $\eta = 1.05$ cp. The robustness of the proposed rupture criterion is firstly re-examined by systematic experiments over a range of parameters to ensure their universal applicability. Another issue of interest is the rupture patterns, which depend strongly on the characteristics of oscillation. We like to emphasize that, even though it seems straightforward to carry out experiments in a more viscous environment, an interesting and distinct pattern of fracture, which differs from the early findings (Li et al. 2012a), is identified. A thorough discussion is presented to categorize these distinct regimes of the chaining instability and their consequences, such as the timings and positions of breakups as well as the possibility of re-attachments after breakups.

A sketch of the experimental apparatus is shown in Fig. 1. In order to form a micro-chain, micro-sized superparamagnetic beads are initially dispersed in a solvent fluid. The solvent fluid used in the experiments is a mixture of distilled water and sodium dodecyl sulfate (SDS) surfactants. The viscosity of this solvent fluid is $\eta = 1.75$ cp. Two types of superparamagnetic beads are used, with a mean diameters of $d = 4.5$ and 2.3 μm whose susceptibilities are $\chi = 1.6$ and 1.0, respectively. A static directional magnetic field, denoted as H_d, is applied to chain the micro-beads. To allow the easy identification of each bead, a chain formed by N beads ($N = 2n + 1$) is labeled from $-n$ to n and the center is denoted as the zeroth bead. It is noticed that, there is no zeroth bead if N is an even number. An additional dynamical field (H_v) is applied perpendicularly, to oscillate the bead chain. This dynamical field is sinusoidal, given by $H_v = H_p\sin(2\pi ft)$, with a maximum field strength H_p and a frequency f. It results in an overall external field of $\mathbf{H} = H_d\,\mathbf{i} + H_v\,\mathbf{j}$, in which $\mathbf{i}$ and $\mathbf{j}$ are unit vectors in the directional (x-direction) and perpendicular (y-direction) axis, respectively. Under the present configuration, the trajectory of the phase angle of the overall external field, denoted as θ_f, is prescribed as $\theta_f(t) = \tan^{-1}[(H_p/H_d)\sin(2\pi ft)]$. The motion of the micro-chain is recorded using an optical microscope that is connected to a digital camera (Silicon Video 643C), whose maximum shooting rate is 200 frames/s. Representative snapshot images, which are modified from the original recorded movies by improving their contrast and resolution, are presented in the following sections to identify the distinct behaviors of micro-chains subjected to various experimental conditions.

2 Results and discussion

2.1 Reference cases

Figure 2 shows images of a representative chain that consists of 15 beads (referred to as a P15 chain therein) subjected to an increasing strength of dynamical field of H_p = 11.44 Oe, 18.73 Oe and 21.83 Oe. The size of the micro-beads is $d = 4.5$ μm. The chaining field strength and the

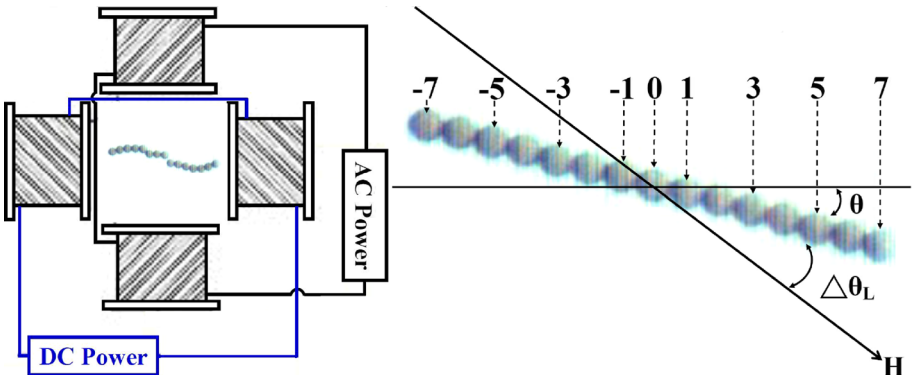

Fig. 1 Principle sketch of experimental setup (*left*) and relevant notations (*right*). A static directional magnetic field provided by DC power is applied to form the chain. An additional sinusoidal dynamical field powered by AC source is applied perpendicularly to oscillate the chain. A chain formed by N particles ($N = 2n + 1$) is labeled from $-n$ to n, whose center is denoted as the zeroth bead. Shown in the figure is a representative P15 chain containing $N = 15$ beads. The phase angle difference between the overall external field (**H**) and the chain is represented by $\Delta\theta_L$

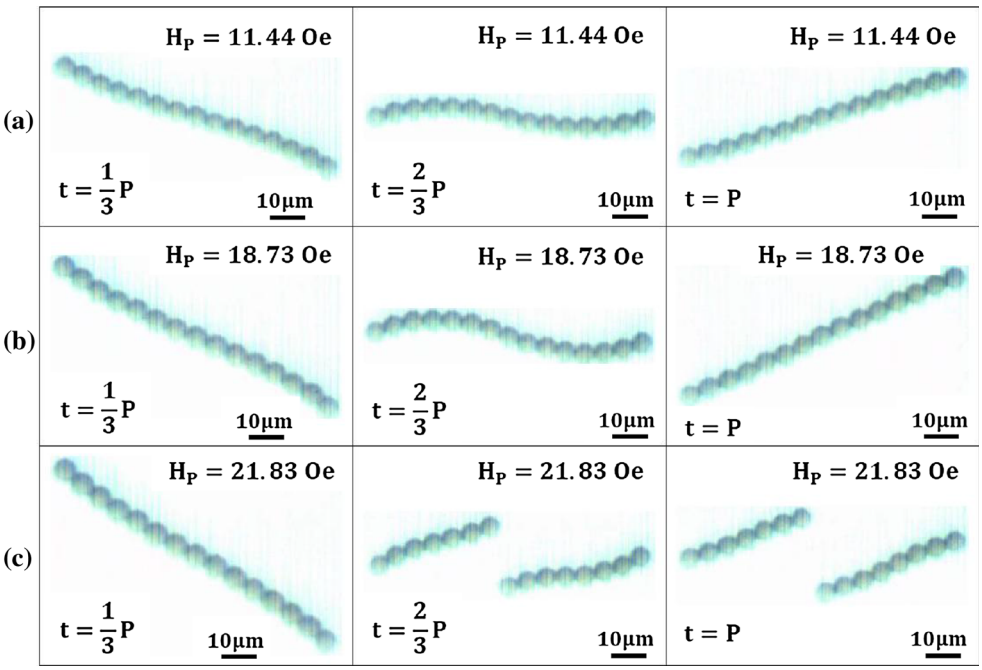

Fig. 2 Sequential images of a chain consisted of 15 beads (P15 chain) subjected to an increasing dynamical field strength of **a** H_p = 11.44 Oe, **b** 18.73 Oe and **c** 21.83 Oe, at different times $t = P/3$, $2P/3$ and $1P$ within a period (P = 1 s in the experiments). The directional field strength and frequency of the oscillating field are H_d = 24.15 Oe and f = 1 Hz, respectively. Critical strength for the dynamical field of 18.73 Oe $< H_p <$ 21.83 Oe is observed to result in a structural rupture of single breakup near center of the chain

oscillating frequency are H_d = 24.15 Oe and f = 1 Hz (or period P = 1 s), respectively. Similar to the results reported in Ref. (Li et al. 2012a), in which less viscous distilled water is used as the solvent fluid, the chain apparently deforms and oscillates consistently under the influence of an overall external field when the field strength is small, e.g., Fig. 2a, b. The amplitude of the oscillation and the prominence of structural deformation become more significant as the field strength increases. If the strength of the dynamical field exceeds a critical value, which is 18.73 Oe $< H_p <$ 21.83 Oe for this case, the chain begins to rupture into two separated segments, as demonstrated in Fig. 2c.

According to the Eqs. (1)–(3) introduced in the previous section, a stronger field strength results in greater torque and leads to more prominent oscillation with a larger amplitude. In the meantime, the instantaneous angular speed is also greater, because of the larger oscillating amplitude within a constant period, so that the induced drag is also greater. Consequently, the chain is ruptured by the induced drag when the field exceeds a certain critical strength. We like to point out that distinct patterns of the present experiments, compared with the previous situations in a less viscous fluid (Li et al. 2012a), are distinguished. Due to more significant viscous drag in the present condition, the critical field strength and the maximum sustainable amplitude (denoted as θ_{A_max}) are much lower than those reported for less viscous distilled water (Li et al. 2012a). The much lower sustainable oscillating amplitude of the chain, e.g., $\theta_{A\_max} < 30°$ (or $\pi/6$), is also demonstrated by the comprehensive phase angle trajectories shown in Fig. 3. The lower amplitude in a more viscous environment is in line with common expectation. Nevertheless, the pattern of a single breakup at a position near middle of the chain is distinct from the pattern of dual breakups at both sides of the chain commonly observed in a less viscous solvent fluid (Li et al. 2012a).

2.2 Effects of controlling parameters

The effect of various controlling parameters, such as the number (N) and the diameter (d) of the beads in the chain and the directional field strength (H_d), is analyzed to obtain more insights in manipulating the chain. A complete series of experiments, in which the lengths of the chains vary from P13 to P17, are firstly performed using the same manipulating field, i.e. a constant chaining field of H_d = 24.15 Oe and an oscillating frequency of f = 1 Hz that is subjected to an increasing dynamical field strength. The effect of N is generally consistent with the early findings (Li et al. 2012a). A shorter chain results in an oscillation that is more synchronized with the overall external field. The critical strength of dynamical field is also stronger for a shorter chain. The rupture patterns are consistent with those shown in Fig. 2c, in which a single breakup occurs near middle of the chain, rather than the dual breakups (Li et al. 2012a), which will be also presented in the later section.

Selected images from another series of experiments, whose beads are smaller (d = 2.3 μm), are shown in Fig. 4. It is interesting to note the great similarity between this P15 chain (Fig. 4a, b) and the P15 chain that has larger beads (Fig. 2b, c). The strengths of the critical fields are both at

18.73 Oe $< H_p <$ 21.83 Oe with a single breakage near middle of the chain. These similarities are attributed to reductions in the drag and the binding magnetic force. Because of a smaller radius (a) and a lower instantaneous angular speed (ω), a reduction in hydrodynamic drags is easily understood by referring to Eq. (2). The lower instantaneous angular speed is a result of the much smaller amplitude within the same period, which can be seen by comparing the images shown in Figs. 2b and 4a. In the meantime, the lesser susceptibility of $\chi = 1.0$ weakens the binding magnetic force between these smaller beads, as demonstrated by Eq. (1). Consequently, the critical field strength is not altered significantly when the beads are smaller. These characteristic observations are generally valid for the P13 to P17 chains tested.

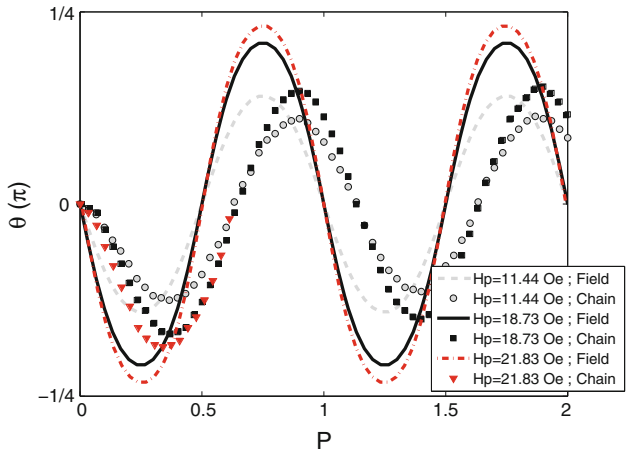

Fig. 3 Phase trajectories within two periods of oscillation of the representative P15 chain shown in Fig. 2. The x-axis denotes the oscillation period ($P = 1$ s). The chain oscillates consistently with the overall external field. Because of viscous dissipation, apparent phase lags are observed. For a sufficient strong field strength of $H_p = 21.83$ Oe, rupture instability is triggered at the phase angle of $\theta \approx 0$, in which the local instantaneous angular speed is maximum

Another parameter that is significant for the manipulation of an oscillating chain is the directional field strength (H_d). In order to evaluate the effect of the chaining field, a series of experiments applying a weaker directional strength of $H_d = 18.15$ Oe were conducted. The size of beads is $d = 4.5$ μm, so that direct comparisons can be made with the cases shown in Fig. 2. Figure 5a–c show the rupture patterns of P13, P15 and P16 chains, respectively. There are apparent differences in the rupture patterns for stronger H_d, as shown in Fig. 2. Because the chaining strength is weaker, the critical field strength is reduced to $H_p = 18.73$ Oe for the same P15 chain. In addition, more unstable patterns of dual breakages are observed for longer chains, e.g., $N \geq 15$. A lower critical strength of the dynamical field is to be expected, since the major role of the directional field is to provide a stable chaining force. Nevertheless, the transition of rupturing patterns that evolves from a single breakage to dual breakages is worthy of further analysis. More discussion of the different patterns of rupture instability is presented in a later section.

The effect of controlling parameters is summarized by their corresponding phase angle trajectories, as shown in Fig. 6. These trajectories are plotted at their experimental maximum dynamical field strengths, which sustain a stable chain without rupture instability. All of the chains oscillate consistently with the overall external field, e.g., at an identical frequency of $f = 1$ Hz. In a fixed field configuration, a shorter chain can be stably manipulated to achieve a more prominent oscillation because of less viscous drag. However, the maximum amplitude of a stable oscillating chain containing the same number of beads is predominantly affected by the directional field strength. A stronger directional field results in a higher critical strength of the dynamical field and allows a more effective manipulation of the micro-chain. Minimum oscillating amplitude is resulted by a chain that consists of smaller beads, because the magnetic susceptibility is smaller.

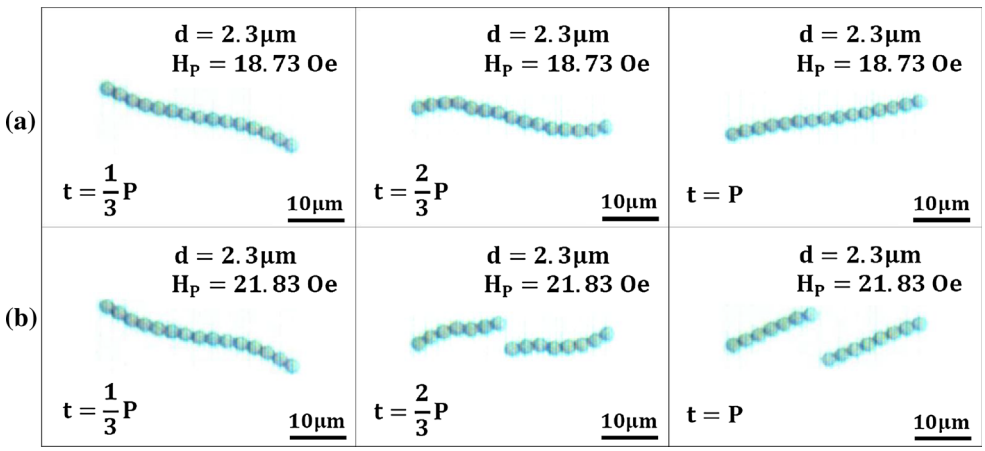

Fig. 4 Sequential images of a P15 chain consisted of smaller beads ($d = 2.3$ μm) subjected to an increasing dynamical field strength of **a** $H_p = 18.73$ Oe and **b** 21.83 Oe. The directional field strength and oscillating frequency are identical to the cases shown in Fig. 2. The overall patterns of oscillation and rupture appear great similarities with the chain consisted of bigger beads

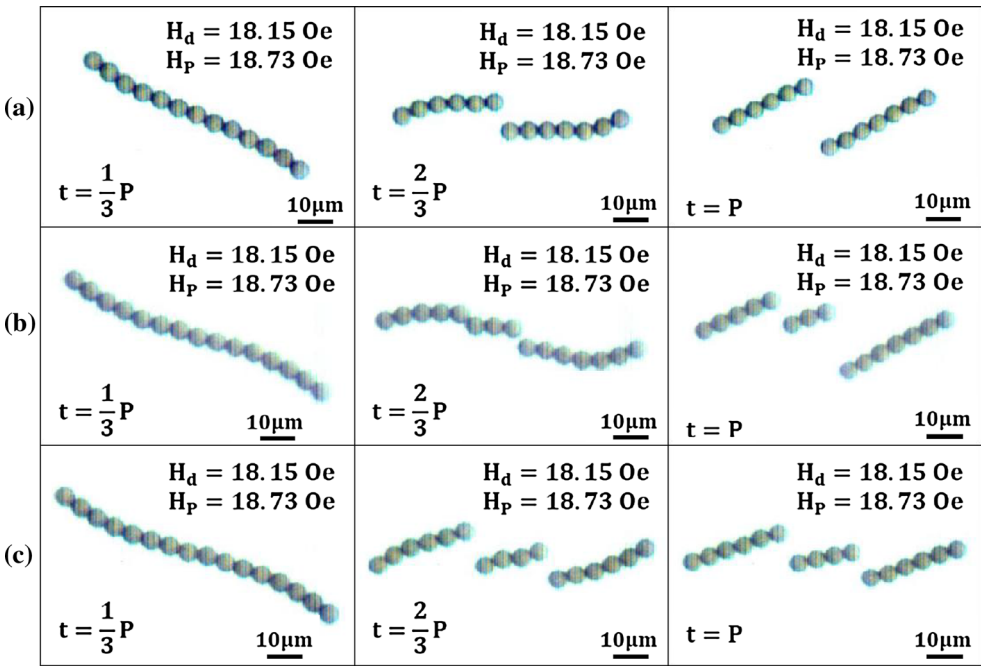

Fig. 5 Sequential images of **a** P13, **b** P15 and **c** P16 chains at a weaker directional field strength of H_d = 18.15 Oe. Less stable chaining structures by a weaker directional field can be realized by the direct comparison between the present condition of a ruptured P15 chain in (**b**) and a stable chain in a stronger directional field shown in Fig. 2b. In addition, chain ruptures evolve from a single breakup near the center in a shorter P13 chain to a more unstable mode of dual breakups in both the P15 and P16 chains

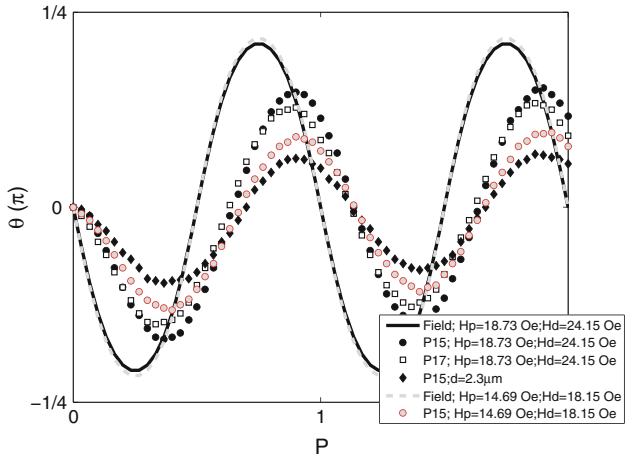

Fig. 6 Phase trajectories of cases with various controlling parameters, i.e. number (N) and size (d) of beads and directional field strength (H_d), at their experimented maximum stable dynamical field strengths. Except the case of d = 2.3 μm, whose correspondent images are shown in Fig. 4a, all the experiments use beads of d = 4.5 μm. Subjected to the same directional field strength, a shorter chain oscillating in larger amplitude is expected due to its smaller induced drag. On the other hand, less pronounced oscillations by chains consisted of smaller beads or subjected to a smaller field are attributed to their weaker magnetization strengths

In general, all of the oscillating amplitudes are much less than those chains manipulated in less viscous distilled water (Li et al. 2012a), which clearly demonstrates the significant effect of the solvent fluid. The significance of the viscous effect is not surprising in such a Stokes regime (Reynolds number $Re \rightarrow 0$), whose length scale is extremely small. In addition, the influences of inertia effects are usually neglected, which can be justified by the sufficiently small value of the Stokes number (St) defined as $St \equiv \frac{T_b}{T_f}$. T_b and T_f stand for the response times of beads and fluid, respectively. Since the Reynolds number is very small in the present condition, the response time of a single bead can be expressed as $T_b = (\rho_b d^2)/(18\eta)$ (Crowe et al. 2012), where ρ_b is the density of bead. By plugging the numerical values of correspondent properties, the beads' response time is in an order of $T_b \sim (10^{-6})$ s. In addition, the solvent fluids are initially stationary and only slow flow induced by the movement of beads, so that the fluid response time can be approximated by the oscillating period P, i.e., $T_f \sim 1$ s. These result in a condition of $St \rightarrow 0$, so that the inertia effects are commonly not considered.

The criterion for chaining instability is examined for various controlling parameters. Because of the transient nature of the oscillating field, the instantaneous values of the Mason number within a period of oscillation vary significantly. It is noticed that the values of time-dependent instantaneous angular speeds ω are obtained by taking the derivatives of the phase angle trajectories and then applied to calculate the numerical value of the Mason number. The values of $Mn^{1/2}*N$ before ruptures in their corresponding critical field conditions are plotted in Fig. 7a. The rupture instabilities all occur at the moment when $Mn^{1/2}*N > 1.7$. It is noticed that numerous experiments are performed for each condition, and the results are all very consistent. These results are in good agreement with the proposed critical value of $Mn^{1/2}*N \approx 1.7$ in Li et al. (2012a), so the proposed criterion is verified more generally. As a result, the stability criterion can be universally applied to chains

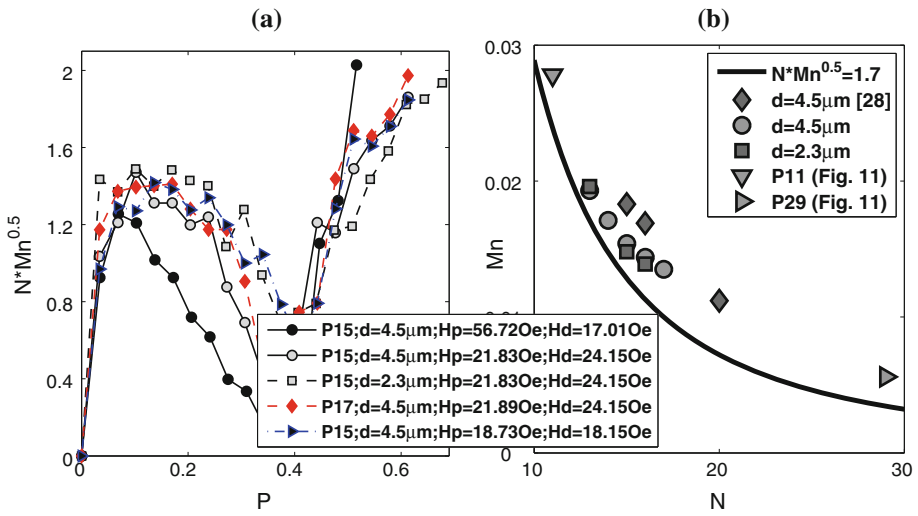

Fig. 7 **a** Evolutions of the numerical values of $Mn^{1/2}*N$ before breakups in various controlling parameters before ruptures. The transient nature of the present oscillating field results in temporal variation of the Mason number within oscillation. The experiment represented by the *solid circle* is conducted in a much less viscous distilled water. The chaining structures cannot be sustained immediately after the $Mn^{1/2}*N$ raised beyond a critical value of $Mn^{1/2}*N \approx 1.7$, which agrees with the criterion proposed in Li et al. (2012a). **b** Phase diagram of the rupture instability. The chains are ruptured if the manipulating conditions exceed the stable criterion of $Mn^{1/2}*N = 1.7$

that contain beads of different sizes (or magnetic susceptibility), or which are manipulated in a more viscous solvent fluid.

To conclude this section, interesting facts regarding the coupling relationship between these two crucial parameters *Mn* and *N* are emphasized. In the common situations of a rational field, the field strength and the angular speed are constant and known, so that *Mn* is independent on *N*. In the present cases, the actual amplitudes of oscillations, which affect the instantaneous angular speeds, result from the interactions of magnetic torques and drags. As a result, value of *Mn* depends strongly on *N* and cannot be predetermined. In general, for a fixed field less prominent oscillation is resulted by a longer chain because of more severe energy dissipation. Consequently, value of the instantaneous Mason number is smaller. In the other word, the coupling effects have been included in the dynamic feature of the instantaneous Mason number. This explains that, even there exists strongly coupling effect between *Mn* and *N*, the chaining stability follows the proposed criterion consistently. Shown in Fig. 7b is the phase diagram of the rupture instability plotted by the two controlling parameters. For the cases tested in various conditions, the chaining instability is triggered immediately after the critical criterion is reached.

2.3 Patterns of chaining instability and reversed rupture

In the previous section, the global criterion to determine the occurrence of rupture instability is generally verified, but this criterion provides no direct information regarding the rupture patterns, which mainly depend on the local dynamics. The topologies of the rupture patterns are important to their application. Kang et al. (2007) argued that the rupture and reattachment of rotating chains lead to more efficient mixings. However, breakages in the oscillating chains significantly reduce the swimming efficiency of micro-swimmers (Li et al. 2013c). In the worst case, the ruptured segments may not rejoin to the original chaining formation and the linear chaining structure is permanently damaged. This indicates that understandings of the local phenomena for chaining instability are not trivial issues.

For a rotational field, a single breakage near middle of the chain to form two separated segments is commonly observed (Petousis et al. 2007; Melle et al. 2003; Melle and Martin 2003; Biswal and Gast 2004). Melle and Martin (2003) suggested that the possibility of brittle or ductile chain fracture depends on the permeability of the particles. Petousis et al. (2007) also reported that the variation in local susceptibility, which can be caused by defects of non-uniformity, alters the positions of a rupture. Detailed simulations (Kang et al. 2007; Gao et al. 2012) demonstrate that multiple breakages can occur for intermediate values of the Mason number. Based on these studies, it is commonly concluded that the chains in a rotational field develop a stable antisymmetric S-shape in a sufficiently low value of the Mason number, or rupture occurs in the vicinity of the chain center if the Mason number exceeds a critical value. On the other hand, Li et al. (2012a, 2013b) reported a distinct pattern of structural instability when a

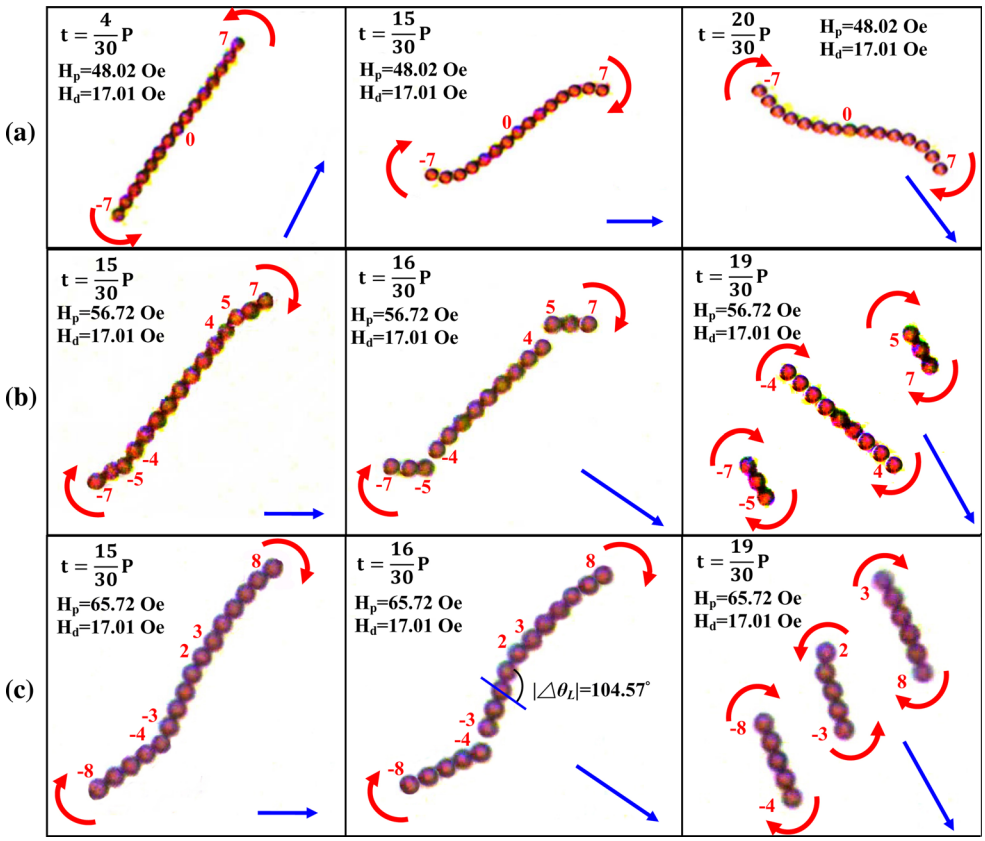

Fig. 8 Typical patterns of a chain with significant oscillating amplitude in distilled water (Li et al. 2012a). Pointing direction and length of the arrow represent orientation and strength of the instantaneous overall external field, respectively. Particular beads are labeled by *number* to indicate their initial positions in the chain. **a** Pattern of a stable S-shaped chain. **b** Weak ductile fracture when dynamical field strength exceeds a certain critical value. Rupture pattern of dual breakups occurs at two sides of the chain. **c** Pattern of dual breakups associated with a reverse oscillation of the middle segment, referred to as the reversed rupture, in even stronger field strength. The instantaneous phase lag of the middle segment is greater than $\pi/2$ to trigger the reversed rupture

chain oscillates in less viscous distilled water. Because the solvent fluid is less viscous, much greater dynamical field strengths (H_p) are sustainable for a stable chain to achieve an oscillation with a significant amplitude. These experiments are re-examined, as shown in Fig. 8, to make comparisons with the present condition of a less prominent oscillation.

Under the influences of a strong dynamical field, e.g., H_p = 48.02 Oe and H_d = 17.01 Oe, Fig. 8a shows a stable chain significantly bent to an S-shape in a less viscous environment. It is noticed that the oscillating orientation begins in a counterclockwise direction in this case, which is opposite to the cases shown in the previous sections. If the dynamical field strength is raised to exceed the critical value, e.g., H_p = 56.72 Oe and 65.72 Oe shown in Fig. 8b, c, respectively, ruptures with dual breakages mainly occur at $t \approx P/2$ toward both sides of the chain, in which the length of middle segment is comparable or even longer than ruptured segments on the sides. In addition, deformation of the oscillating chains is very insignificant before these ruptures. Compared with the ruptured chains in a more viscous solvent fluid presented in the previous sections, the motions of these chains appear to be more rigid before the dual breakages occur, so the pattern of instability is more appropriately referred to as a weak ductile fracture. In common unstable cases, the broken segments periodically undergo processes of re-chaining and rupture. However, an unconventional rupture phenomenon is also observed, in which the oscillating directions are inconsistent between the broken segments, as shown in Fig. 8c. This pattern of counter-oscillating segments is referred to as a reversed rupture. The reason for this reversed rupture is a local trajectory shift in the central segment. Because there is bending deformation on two sides of the chain, the local phase lag to the overall external field in the central region is the greatest. It is possible that this maximum phase lag can exceed $\pi/2$, which results in a shift in the local trajectory (Li et al. 2013a) and an oscillation opposite to the overall external field. If the outer segments remain to lag the overall external field by less than $\pi/2$ and continue their original motion, there is counter-oscillation between the segments. As demonstrated in Fig. 8c, this counter-

oscillation between the segments bends the chain and triggers dual breakages at the sides. It is important to note that such a reversed rupture may prevent the broken segments from rejoining linearly and leads to a permanent failure of the chaining structure.

The rupture patterns observed in the experiments with smaller oscillating amplitudes are more toward center of the chain, with either a single breakage or dual breakages, as shown in Figs. 2, 4 and 5. The pattern of a single breakage has been commonly observed in a rotational field, while multiple breakages are rarely reported, except the results by direct numerical simulations and recent experiments (Kang et al. 2007; Gao et al. 2012). The simulations reveal that the rupture patterns evolve from a basic mode of a single breakage at the center of the chain to more chaotic patterns of multiple breakages, when the value of the Mason number increases. There are notable distinctions in the rupture patterns for these cases of smaller oscillating amplitudes and cases of weak ductile fracture, as shown in Fig. 8b, c. Firstly, deformation before rupture is more apparent, and the positions of the breakages are more toward center of the chain. Even in some cases with a similar pattern of dual breakages, the positions are toward the center, which results in a shorter middle segment. In addition, the timings of ruptures are delayed to $t \approx 2P/3$. These differences suggest that the chaining instability is in a different regime, referred to as a strong ductile fracture because of an apparent deformation before rupture. The detailed dynamics of the regimes for weak and strong ductile fractures are discussed in the following paragraphs.

2.3.1 Weak ductile fracture

A weak ductile fracture, e.g., patterns shown in Fig. 8, which features dual breakages at the outer regions of the chain, in which a comparable or even longer middle segment is formed after the rupture, is favored when there is a pronounced oscillation of large amplitude. Even though the maximum amplitude is given by $\theta_{\max} = \tan^{-1}(H_p/H_d)$, the actual amplitude is reduced by viscous dissipation. As a result, a strong dynamical field strength in a less viscous fluid is essential to achieve a pronounced oscillation. For typical experiments shown in Fig. 8, the actual oscillating amplitudes are measured as $\theta_{A\_max} \approx 70°$, compared with $\theta_{A\_max} < 30°$ in a more viscous condition presented in the previous section. In this situation, the overall angular speed is faster, compared with the cases in a more viscous condition, associated with a rapid variation within an oscillating period. This significant speed variation constrains a prominent stable deformation before rupture. In addition, the strength of the overall field also appears to vary significantly, i.e., a maximum of $H = \sqrt{(H_p{}^2 + H_d{}^2)}$ at $t = P/4$ and a minimum of $H = H_d$ at $t = P/2$. It is natural that the critical condition is determined by the minimum overall field strength, when the bonding magnetic attraction is the weakest. As a result, the most favorable time to trigger the chaining instability is at $t \approx P/2$, when the field strength is the weakest. These facts prove that a weak ductile fracture is preferable to happen at $t \approx P/2$. To further understand the favored position of local ruptures, an analysis of the detailed force distributions that act on the chains is necessary. For a chain of $2n + 1$ beads, labeled from $-n$ to n, whose origin is centered on the zeroth bead, the radial dipolar interaction (F_D) over the ith bead due to the rest of beads in the chain is given by Melle et al. (2000)

$$F_{D_i} = \frac{3\mu_0 m^2}{4\pi}(3\cos^2\Delta\theta_L - 1)\left[\sum_{j=-n}^{i-1}\frac{1}{r_{ij}{}^4} - \sum_{j=i+1}^{n}\frac{1}{r_{ij}{}^4}\right], \qquad (4)$$

where, $r_{ij} = |r_i - r_j| = 2a|i - j|$ is the distance between the centers of the ith and jth beads. These radial dipolar forces are commonly used to determine structural instability (Petousis et al. 2007; Melle et al. 2003; Melle and Martin 2003; Biswal and Gast 2004). Nevertheless, the normal forces acting on the interfaces between the beads, which constrain the mobility of the beads and induce tangential friction in realistic situations, can also play an important role in sustaining chaining structures. The normal force acting on the interface between the $(i - 1)$th and ith beads, denoted as $F_{N_{i-\frac{1}{2}}}$, is depicted in Fig. 9 and is calculated by

$$F_{N_{i-\frac{1}{2}}} = \sum_{j=i}^{n} F_{D_j}. \qquad (5)$$

The typical distribution of the normal forces (F_N) among the beads appears to be the weakest and varies significantly near the sides, which is similar to the trends shown in Fig. 10. It is expected that the friction, denoted F_f, would be directly proportional to the normal force, i.e., $F_f \sim F_N$. Since the actual numerical value of friction coefficient or even its order of magnitude is not presently available, influences of the friction are seldom discussed. Nevertheless, qualitative arguments can be concluded based on the distributions of normal forces between beads. In the situation of more dramatic rupture without significant

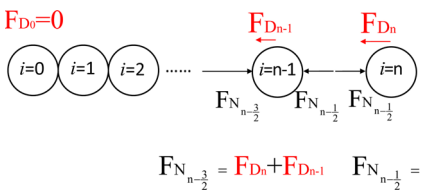

Fig. 9 Principle sketch of dipolar forces (F_D) and normal force (F_N) acting on beads and interfaces, respectively

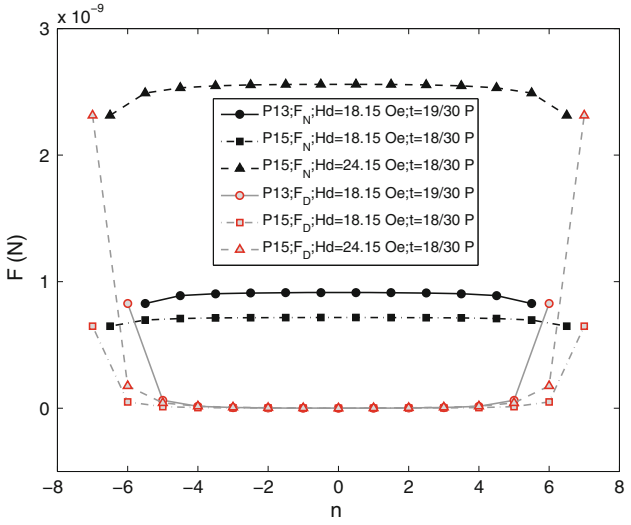

Fig. 10 Distributions of dipolar (F_D) and normal (F_N) forces acting on individual beads immediately before ruptures for the cases of a P15 chain with single breakup, a P13 chain with single breakup and a P15 chain with dual breakups shown in Figs. 2c and 5a, b, respectively. The overall normal forces are the lowest in the case of a longer P15 chain subjected to a weaker directional field strength of $H_d = 18.15$ Oe, which appears a more unstable mode of dual breakups

deformation, i.e., the weak ductile fracture, the facts of weaker normal forces associated with rapid variations near the sides locally provide a qualitative assessment that the positions of breakages favor the outer regions.

2.3.2 *Strong ductile fracture*

On the other hand, oscillations with smaller amplitudes in a more viscous environment commonly lead to the rupture patterns of strong ductile fractures. For the cases presented in the previous section, the amplitudes are usually $\theta_{A\_max} < 30°$ as shown in Figs. 3 and 6. Because of this small amplitude, magnitudes and variations of the instantaneous angular speeds among an oscillating period are both less significant, so the chain is structurally more ductile. A prominent deformation before rupture is allowed. When there is weak field strength and strong viscous drag, the primary factor to determine chaining instability is the variation in the drag. Consequently, the preferred timing for a rupture is at the time of maximum instantaneous angular speed, when the induced drag is greatest. For all of the experimental cases involving a more viscous environment, ruptures occur when the chains orientate almost horizontally, shortly before $t \approx 2P/3$. Examinations of their trajectories show that the breakages occur at the times when the local instantaneous angular speed is maximum, i.e., $\theta \approx 0$ as a representative trajectory before rupture for $H_p = 21.83$ Oe and $H_d = 24.15$ Oe shown in Fig. 3. Numerical simulations for a steady rotational S-shaped chain (Kang et al. 2007) reveal that a counter-rotating vortex pair is generated in the middle region, which leads to a rupture locally. By the same token, a rupture near center of the chain is preferred for strong ductile fractures.

Qualitative observations for strong ductile fractures in the previous section suggest that the rupture patterns are predominantly influenced by the length of the chain and the strength of the directional field, e.g., multiple breakages in a longer chain subjected to a weaker directional field, as shown in Fig. 5. Figure 10 shows a plot of the force distributions for three chains of different lengths and directional field strengths, i.e., $N = 13$, 15 and $H_d = 18.15$ Oe, 24.15 Oe, which are subjected to their corresponding critical dynamical field strengths at a time immediately before rupture. The corresponding images of the P15 chain for $H_d = 24.15$ Oe, the P13 chain in $H_d = 18.15$ Oe and the P15 chain in $H_d = 18.15$ Oe are shown in Figs. 2c and 5a, b, respectively. Figure 10 clearly demonstrates that the overall stabilizing normal forces are weakest for a longer P15 chain that is subjected to a weaker directional field strength of $H_d = 18.15$ Oe. In line with the experimental observations, this particular chain appears to have a more unstable pattern, e.g., dual breakages, as shown in Fig. 5b. These assessments provide a quantitative validation that the pattern for chaining instability is mainly affected by the length of the chain and the strength of the directional field. These findings are also verified by additional experiments involving a weaker directional field strength and a longer chains. Shown in Fig. 11 are sequential images of a P11 chain subjected to a weak directional field strength of $H_d = 3.15$ Oe, and a long P29 chain in $H_d = 14.15$ Oe. Because of a very weak chaining field strength, the P11 chain ruptures into 4 segments right after its movement. On the other hand, an excessive length of the P29 chain results in a more disorder fracture. Their correspondent Mason numbers are plotted in Fig. 7b, which also exceed the critical value. These results also support the fact that multiple breakups is another common rupture pattern in an oscillating chain, which is favorable when longer chains are subjected to a weaker directional field.

3 Concluding remarks

In this study, distinct patterns of fracture instability in an oscillating magnetic micro-chain, which depend strongly on the viscosity of the solvent fluid, are identified and discussed. In order to analyze these particular fracture

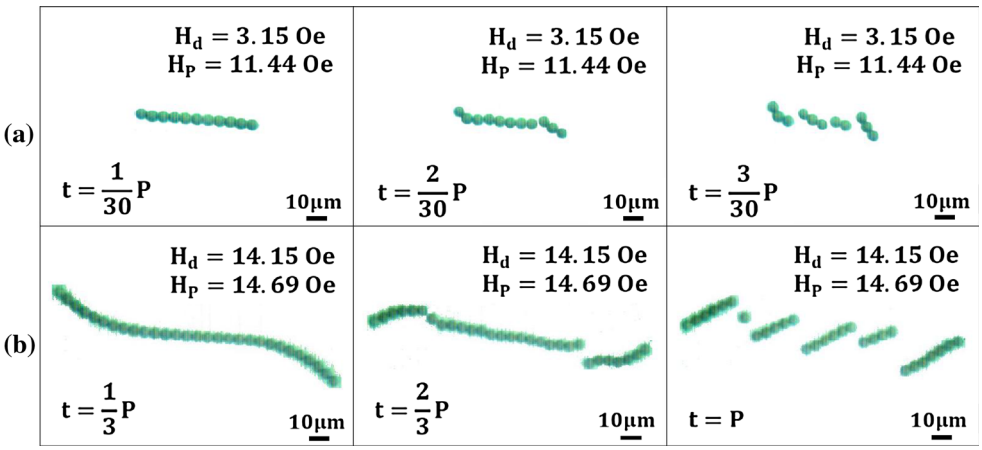

Fig. 11 Sequential images of **a** a P11 chain subjected to a weak directional field strength of H_d = 3.15 Oe, and **b** a long P29 chain in H_d = 14.15 Oe. Because of a very weak chaining field strength, the P11 chain ruptures into 4 segments right after its movement. On the other hand, an excessive length of the P29 chain results in a more disorder fracture

patterns, systematic experiments in a more viscous mixture are first investigated. Because of the significant induced drag, the critical strength of the dynamical field to sustain a stable chaining structure is much lower than for the cases in less viscous distilled water (Li et al. 2012a). In addition, the allowable oscillating amplitudes are also less pronounced. These phenomena result in variations of timings and locations of the chain breakup. Determined by the viscosities of solvent fluids, two distinct regimes, referred to as a weak ductile fracture and a strong ductile fracture, are categorized and discussed in detail.

A weak ductile fracture describes insignificant deformation immediately before chain rupture. This often occurs when the chain experiences a pronounced oscillation of large amplitude. In order to achieve a pronounced oscillation, a strong field in a less viscous solvent fluid is required, such as distilled water (Li et al. 2012a). To further understand the mechanisms at work, the cases in distilled water are revisited and detailed distributions of normal forces acting between the particles and interactions with the induced drag are analyzed. Because of the large amplitude, the temporal variations in both the local instantaneous angular speed and the corresponding induced drag are severe. The chain tends to be broken in a more rigid manner, before apparent deformation. In addition, the distribution of the normal forces between the interfaces of the beads appears to vary more significantly in the outer region, so the positions of rupture usually favor toward the sides of the chain. The preferred time for a rupture is at $t \approx P/2$, when the overall field strength is weakest. An interesting phenomenon of ruptured segments in counter oscillations, referred to as a reversed rupture, is newly identified when there is an excessive dynamical field. This reversed rupture occurs when the phase lag of the middle segment of the chain is greater than $\pi/2$, which triggers a local trajectory shift (Li et al. 2013a). An important consequence of this reversed rupture is that broken segments may be prevented from rejoining and lead to permanent failure of a linear chaining structure.

A strong ductile fracture, which features significant deformation before rupture, is favorable in a more viscous solvent fluid, in which pronounced oscillation is difficult to achieve. In contrary to a weak ductile fracture, the positions of breakages are toward the middle region of the chain, because the vortex pairs are generated by an S-shaped deformation. The experimental results suggest that the rupture patterns are mainly influenced by two factors: the length of the chain and the strength of the directional field. The prominence of rupture instability, which can be represented by the number of breakages in the chain, is enhanced in a weaker directional field or a longer length. These experimental observations are in line with quantitative assessments determined by the distributions of normal forces.

Finally, supplementary but non-trivial results of the experiments conducted in different manipulating conditions provide further validations of the global criterion for rupture instability, given by $Mn^{1/2}*N \approx 1.7$ which was initially proposed based on the measurements for pure distilled water (Li et al. 2012a).

Acknowledgments This study was financially supported by the National Science Council of Republic of China (Taiwan) through Grant NSC 99-2221-E-009-057-MY3.

References

Banerjee U, Bit P, Ganguly R, Hardt S (2012) Aggregation dynamics of particles in a microchannel due to an applied magnetic field. Microfluid Nanofluid 13:565

Biswal S, Gast A (2004) Rotational dynamics of semiflexible paramagnetic particle chains. Phys Rev E 69:041406

Biswal S, Gast A (2004) Micromixing with linked chains of paramagnetic particles. Anal Chem 76:6448

Cebers A (2005) Flexible magnetic filaments. Curr Opin Colloid Interface Sci 10:167
Cebers A (2005) Flexible magnetic swimmer. Magnetohydrodynamics 41:63
Cebers A, Javaitis I (2004) Dynamics of a flexible magnetic chain in a rotating magnetic field. Phys Rev E 69:021404
Cebers A, Ozols M (2006) Dynamics of an active magnetic particle in a rotating magnetic field. Phys Rev E 73:021505
Crowe C, Schwarzkopf J, Sommerdeld M, Tsuji Y (2012) Multiphase flows with droplets and particles, 2nd edn. CRC Press, Boca Raton
Dreyfus R, Baudry J, Roper M, Fermigier M, Stone H, Bibette J (2005) Microscopic artificial swimmers. Nature 437:862
Erglis K, Zhulenkovs D, Sharipo A, Cebers A (2008) Elastic properties of DNA linked flexible magnetic filaments. J Phys Condens Matter 20:204107
Frka-Petesic B, Erglis K, Berret JF, Cebers A, Dupuis V, Fresnais J, Sandre O, Perzynski R (2011) Dynamics of paramagnetic nanostructured rods under rotating field. J Magn Magn Mater 323:1309
Gao Y, Hulsen MA, Kang TG, den Toonder JMJ (2012) Numerical and experimental study of a rotating magnetic particle chain in a viscous fluid. Phys Rev E 86:041503
Goubault C, Jop P, Fermigier M, Baudry J, Bertrand E, Bibette J (2003) Flexible magnetic filaments as micromechanical sensors. Phys Rev Lett 91:260802
Kang TG, Hulsen M, Anderson P, den Toonder JMJ, Meijer H (2007) Chaotic mixing induced by a magnetic chain in a rotating magnetic field. Phys Rev E 76:066303
Karle M, Wohrle J, Miwa J, Paust N, Roth G, Zengerle R, von Stetten F (2011) Controlled counter-flow motion of magnetic bead chains rolling along microchannels. Microfluid Nanofluid 10:935
Lacharme F, Vandevyver C, Gijs M (2009) Magnetic beads retention device for sandwich immunoassay comparison of off-chip and on-chip antibody incubation. Microfluid Nanofluid 7:479
Li Y-H, Chen C-Y, Sheu S-T, Pai J-M (2012a) Dynamics of a microchain of superparamagnetic beads in an oscillating field. Microfluid Nanofluid 13:579
Li Y-H, Sheu S-T, Pai J-M, Chen C-Y (2012b) Manipulations of oscillating micro magnetic particle chains. J Appl Phys 111:07A924
Li Y-H, Lin H-C, Chen C-Y (2013a) Trajectory shift of magnetic microchains in an oscillating field. Microfluid Nanofluid 14:831
Li Y-H, Bansal E, Chen C-Y (2013b) Breakups of magnetic chains in an oscillating field. Magnetohydrodynamics (accepted)
Li Y-H, Lin H-C, Chen C-Y (2013c) Steering of magnetic microswimmers. IEEE Trans Magn 49(7):4120
Melle S, Martin JE (2003) Chain model of a magnetorheological suspension in a rotating field. J Chem Phys 118:21
Melle S, Fuller G, Rubio M (2000) Structure and dynamics of magnetorheological fluids in rotating magnetic fields. Phys Rev E 61:4111
Melle S, Calderon O, Fuller G, M. Rubio (2002a) Polarizable particle aggregation under rotating magnetic fields using scattering dichroism. J Colloid Interface Sci 247:200
Melle S, Calderon O, Rubio M, Fuller G (2002b) Rotational dynamics in dipolar colloidal suspensions: video microscopy experiments and simulations results. J Non-Newton Fluid Mech 102:135
Melle S, Calderon OG, Rubio MA, Fuller GG (2003) Microstructure evolution in magnetorheological suspensions governed by Mason number. Phys Rev E 68:041503
Nguyen NT (2012) Micro-magnetofluidics: interactions between magnetism and fluid flow on the microscale. Microfluid Nanofluid 12:1
Petousis I, Homburg I, Derks R, Dietzel A (2007) Transient behaviour of magnetic micro-bead chains rotating in a fluid by external fields. Lab Chip 7:1746
Roy T, Sinha A, Chakraborty S, Ganguly R, Puri I (2009) Magnetic microsphere-based mixers for microsroplets. Phys Fluids 21:027101
Vuppu A, Garcia A, Hayes M (2003) Video microscopy of dynamically aggregated paramagnetic particle chains in an applied rotating magnetic field. Langmuir 19:8646
Weddemann A, Wittbracht F, Auge A, Hutten A (2011) Particle flow control by induced dipolar interaction of superparamagnetic microbeads. Microfluid Nanofluid 10:459
Wittbracht F, Weddemann A, Eickenberg B, Hutten A (2012) On the direct employment of dipolar particle interaction in microfluidic system. Microfluid Nanofluid 13:543